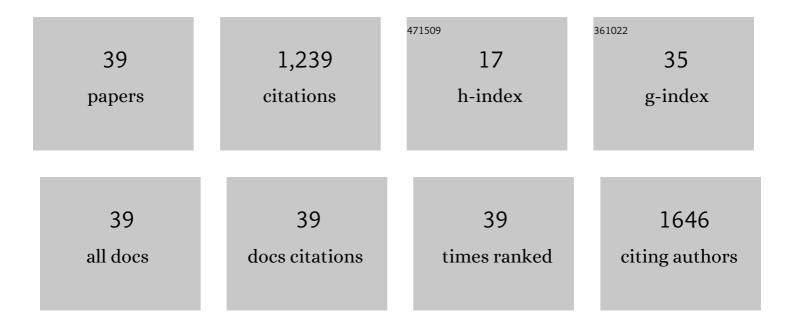
Shufang Wang

List of Publications by Year in descending order

Source: https://exaly.com/author-pdf/5043342/publications.pdf Version: 2024-02-01



#	Article	IF	CITATIONS
1	ds-Block Element-Enabled Cooperative Regulation of Electrical and Thermal Transport for Extraordinary N- and P-Type PbSe Thermoelectrics near Room Temperature. Chemistry of Materials, 2022, 34, 1862-1874.	6.7	8
2	Coke and sintering resistant nickel atomically doped with ceria nanosheets for highly efficient solar driven hydrogen production from bioethanol. Green Chemistry, 2022, 24, 2044-2050.	9.0	14
3	Ultrahigh in-plane thermoelectric performance in self-assembled PbSe:Au films with vertically aligned nanopillars. Acta Materialia, 2022, 227, 117692.	7.9	4
4	Unveiling the advantages of an ultrathin N-doped carbon shell on self-supported tungsten phosphide nanowire arrays for the hydrogen evolution reaction experimentally and theoretically. Nanoscale, 2022, 14, 5430-5438.	5.6	14
5	Weak sunlight-driven mass toluene combustion through scalable Cu doped CeO2 microspheres. Journal of Cleaner Production, 2021, 293, 125328.	9.3	4
6	Sewage-free preparation of 2D metal oxides by a rapid freezing soft template method for extraordinarily activating solar-driven humidity VOC combustion. Catalysis Science and Technology, 2021, 11, 2456-2460.	4.1	6
7	Solar-heating thermocatalytic H ₂ production from formic acid by a MoS ₂ -graphene-nickel foam composite. Green Chemistry, 2021, 23, 7630-7634.	9.0	7
8	Efficient hydrogen production <i>via</i> sunlight-driven thermal formic acid decomposition over a porous film of molybdenum carbide. Journal of Materials Chemistry A, 2021, 9, 22481-22488.	10.3	9
9	Lateral photovoltaic effect based on novel materials and external modulations. Journal Physics D: Applied Physics, 2021, 54, 153003.	2.8	11
10	Ambient sunlight-driven photothermal methanol dehydrogenation for syngas production with 32.9 % solar-to-hydrogen conversion efficiency. IScience, 2021, 24, 102056.	4.1	12
11	Surprisingly high in-plane thermoelectric performance in a-axis-oriented epitaxial SnSe thin films. Materials Today Physics, 2021, 18, 100399.	6.0	17
12	The <i>in situ</i> removal of surface molybdenum oxide for making binder-free porous Mo _{1.98} C _{1.02} film a more efficient electrocatalyst for alkaline rather than acidic hydrogen production. Sustainable Energy and Fuels, 2021, 5, 3373-3381.	4.9	4
13	Ni loaded on N-doped carbon encapsulated tungsten oxide nanowires as an alkaline-stable electrocatalyst for water reduction. Sustainable Energy and Fuels, 2020, 4, 788-796.	4.9	15
14	A 2D-SnSe film with ferroelectricity and its bio-realistic synapse application. Nanoscale, 2020, 12, 21913-21922.	5.6	28
15	Efficient combustion of chlorinated volatile organic compounds driven by natural sunlight. Science of the Total Environment, 2020, 749, 141595.	8.0	14
16	Outdoor sunlight-driven scalable water-gas shift reaction through novel photothermal device-supported CuO _x /ZnO/Al ₂ O ₃ nanosheets with a hydrogen generation rate of 192 mmol g ^{â^'1} h ^{â^'1} . Journal of Materials Chemistry A, 2020, 8, 19467-19472.	10.3	23
17	Triple Functions of Ni(OH) ₂ on the Surface of WN Nanowires Remarkably Promoting Electrocatalytic Activity in Full Water Splitting. ACS Catalysis, 2020, 10, 13323-13333.	11.2	120
18	Laser-induced photoresistance effect in Si-based vertical standing MoS ₂ nanoplate heterojunctions for self-powered high performance broadband photodetection. Journal of Materials Chemistry C, 2019, 7, 10642-10651.	5.5	24

SHUFANG WANG

#	Article	IF	CITATIONS
19	Mass production of superhydrophilic sponges for efficient and stable solar-driven highly corrosive water evaporation. Environmental Science: Water Research and Technology, 2019, 5, 2041-2047.	2.4	5
20	Significant enhancement of energy storage density and polarization in self-assembled PbZrO ₃ : NiO nano-columnar composite films. Nanoscale, 2019, 11, 1914-1920.	5.6	22
21	Significant average <i>ZT</i> enhancement in Cu ₃ SbSe ₄ -based thermoelectric material <i>via</i> softening p–d hybridization. Journal of Materials Chemistry A, 2019, 7, 17648-17654.	10.3	41
22	Selective light absorber-assisted single nickel atom catalysts for ambient sunlight-driven CO2 methanation. Nature Communications, 2019, 10, 2359.	12.8	185
23	Fe3Si assisted Co3O4 nanorods: A case study of photothermal catalytic CO oxidation under ambient solar irradiation. Nano Energy, 2019, 62, 653-659.	16.0	36
24	A vertically layered MoS ₂ /Si heterojunction for an ultrahigh and ultrafast photoresponse photodetector. Journal of Materials Chemistry C, 2018, 6, 3233-3239.	5.5	132
25	Ultrahigh, Ultrafast, and Selfâ€Powered Visibleâ€Nearâ€Infrared Optical Positionâ€5ensitive Detector Based on a CVDâ€Prepared Vertically Standing Few‣ayer MoS ₂ /Si Heterojunction. Advanced Science, 2018, 5, 1700502.	11.2	87
26	The transverse thermoelectric effect in <i>a</i> -axis inclined oriented SnSe thin films. Journal of Materials Chemistry C, 2018, 6, 12858-12863.	5.5	14
27	Synthesis of mesoporous Fe ₃ Si aerogel as a photo-thermal material for highly efficient and stable corrosive-water evaporation. Journal of Materials Chemistry A, 2018, 6, 23263-23269.	10.3	23
28	Microstructure and thermoelectric transport properties of BiCuSeO thin films on amorphous glass substrates. Dalton Transactions, 2018, 47, 11091-11096.	3.3	1
29	Synthesizing new types of ultrathin 2D metal oxide nanosheets via half-successive ion layer adsorption and reaction. 2D Materials, 2017, 4, 025031.	4.4	18
30	Ultrahigh, ultrafast and large response size visible-near-infrared optical position sensitive detectors based on CIGS structures. Journal of Materials Chemistry C, 2017, 5, 4915-4922.	5.5	40
31	Large Lateral Photovoltage Observed in MoS ₂ Thickness-Modulated ITO/MoS ₂ /p-Si Heterojunctions. ACS Applied Materials & Interfaces, 2017, 9, 18377-18387.	8.0	68
32	Enhanced polarization and dielectricity in BaTiO ₃ :NiO nanocomposite films modulated by the microstructure. RSC Advances, 2017, 7, 38231-38242.	3.6	7
33	Passivation of defect states in anatase TiO2 hollow spheres with Mg doping: Realizing efficient photocatalytic overall water splitting. Applied Catalysis B: Environmental, 2017, 202, 127-133.	20.2	117
34	Growth of <i>c</i> â€Axisâ€Oriented BiCuSeO Thin Films Directly on Si Wafers. Journal of the American Ceramic Society, 2016, 99, 3367-3370.	3.8	12
35	Light-induced transverse voltage effect in c-axis inclined BiCuSeO single crystalline thin films. Optical Materials Express, 2016, 6, 558.	3.0	14
36	The Reverse Lateral Photovoltaic Effect in Boron-Diffused Si p-n Junction Structure. IEEE Electron Device Letters, 2016, 37, 201-204.	3.9	14

#	Article	IF	CITATIONS
37	Epitaxial growth and thermoelectric properties of c-axis oriented Bi _{1â^'x} Pb _x CuSeO single crystalline thin films. CrystEngComm, 2015, 17, 8697-8702.	2.6	18
38	The enhancement of photo-thermo-electric conversion in tilted Bi_2Sr_2Co_2Oy thin films through coating a layer of single-wall carbon nanotubes light absorber. Optics Express, 2013, 21, 18336.	3.4	11
39	Laser-induced voltage characteristics of Bi2Sr2Co2Oy thin films on LaAlO3 substrates. Applied Surface Science, 2010, 257, 157-159.	6.1	40